AERODYNAMIC TECHNOLOGY INTEGRATION ON THE TP400 AND E3E CORE COMPRESSORS

V. Gümmer, R. Digele, T. Gietl

Rolls-Royce Deutschland Ltd. & Co. KG
Eschenweg 11, D-15827 Blankenfelde-Mahlow
Germany

OVERVIEW

Modern axial compressor stages need to be designed at increasingly higher aerodynamic stage loading, while the performance required has to be improved further. A new family of compressors has been developed over the past years incorporating novel aerofoil concepts and taking into account the strongly three-dimensional character of the flow field. In an approach of building a family of highly efficient compressors for a range of various applications and pressure ratios, the TP400 and Engine3E (E3E) core compressors were designed and tested. Integrating the technology of these two machines the E3E compressor achieved a pressure ratio and efficiency in only nine stages, which is unique for contemporary designs.

The present paper describes the general family concept, the elements of technology being integrated, and also some results of numerical design studies as well as test results of both compressors. The performance of compressors with reduced stage count and increased loading is primarily determined by three-dimensional end wall flow phenomena. Therefore, special emphasis is put on the numerical analysis of aerofoil features and cavities along the boundaries of the main flow path, which represent the challenging elements of the design.

1. INTRODUCTION

The compression system of an aero-engine has a high potential to contribute to weight and cost reduction of the unit. In order to allow the desired reduction in stage and part count, the aerodynamic loading of the individual blade rows must rise, but highly-loaded compressors can only be designed for high efficiency if the boundary layers on both aerofoil and end wall are well controlled.

In the eighties controlled-diffusion aerofoils were introduced to control the two-dimensional profile boundary layers [1], [2]. In the nineties the deliberate use of sweep and dihedral was widely explored and applied to a number of compressor designs [3], [4], [5], [6].

At the loading level given on modern axial compressors the performance largely depends on the three-dimensional secondary flows occuring in the end wall regions. Further enhancement of the design can be achieved by a new generation of 3D aerofoils, the tailoring of geometry details along the boundaries of the flow path, such as fillet radii, shroud wells, bleed off-takes/cavities and radial clearances.

2. PRODUCT REQUIREMENTS

Over the last decade requirements for reduction of fuel burn, reduction of operating cost and increased time-on-wing have driven engine manufacturers to consider ambitious enhancements of the engine thermodynamic cycle and architecture, and the component performance. Therefore, fan bypass ratios have increased, and as a consequence the core compressor module reduced in size, implying a more difficult mechanical design and control of tip clearances. On the other hand compressor pressure ratio and efficiency had to rise, whereas module weight, cost and mechanical complexity had to reduce.

FIG 1 shows the E3E and the TP400 core compressor modules and the main design goals. Both compressors are highly loaded, feature a low number of variable stator vanes for the given pressure ratio and have been weight-optimised using rotor blisk design across most of the stages. The TP400 compressor inlet flow size is significantly below that of the E3E compressor. However, both compressors meet the aggressive surge margin and polytropic efficiencies targets.

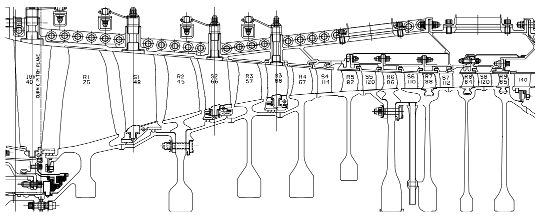

E3E Core Compressor

TP400 Core Compressor

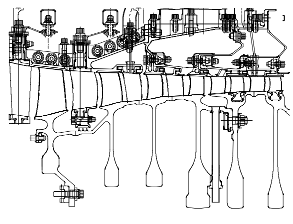

	TP400	E3E
Pressure Ratio [-]	>6	>20
Corrected Flow Size [lb/s]	26	65
No. of Stages	6	9

FIG 1. Compressor General Arrangements

3. AERODYNAMIC DESIGN

The E3E and the TP400 core compressors were developed during the period of 2002 to 2006. The 9-stage E3E compressor was validated through a programme of two rig builds tested in late 2003 and mid 2006 funded by the Brandenburg state. The 6-stage TP400 compressor was designed in 2004 and tested in late 2005 on only one rig build. The design process for both compressors included a standard S1S2 procedure complemented with high-fidelity CFD predictions, which allowed to meet the design goal in one iteration on the E3E compressor and to have a first-time-right design on the TP400 compressor. The trend to be observed on the number of rig tests reducing from approximately 10 in the eighties down to 1 or 2 today is achieved through a continuous and successful improvement of design process and tools.

3.1. Core Compressor Strategy

The E3E compressor was design-optimised to meet requirements of the future generation of two-shaft engines in the thrust range of the existing AE3007, BR700 and V2500 engines. The individual compressor flow sizes and pressure ratios considered for engines in the respective business and regional jet thrust range are obtained by simply scaling the flow path and the aerodynamics of the E3E demonstrator (master). Compressor configurations with reduced pressure ratio are derived by removing stages (de-staging) the 9-stage master configuration. The compressor was developed on the basis of the well-known BR700 series [7]. However, significant changes had to be introduced to meet future performance goals [8]. To achieve this, both blade speed and stage loading was increased to a level well beyond that of the BR700. Stage count was reduced by one but pressure ratio was increased from 16 to above 20. In order to accommodate the increased pressure ratio the annulus was optimised using aerodynamic and mechanical constraints.

The 6-stage core compressor of the TP400 turboprop has a different mission profile to the two-shaft engine core compressors. There is an extremely wide range of cruise conditions to cover with good efficiencies, and also cruise, climb and take-off strongly differ in flow. However, the geometric and aerodynamic design parameters of the TP400 compressor are tightly within the design envelopes of the E3E compressor. The inner block of stages 3 to 8 of the E3E compressor suits the TP400 design objectives and therefore provided a solid baseline when defining the 6-stage TP400 compressor, see FIG 2.

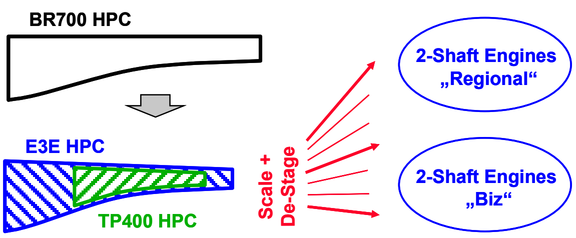

FIG 2. Core Compressor Strategy

3.2. Major Design Choices

Relative to the BR700 compressor introduced into service in 1996 the E3E compressor was designed to significantly higher loadings, and due the high overall pressure ratio also the flow path had to feature stronger slopes along the hub and casing. A more falling casing line was required to account for limitations in rotor hub-to-tip ratio at the front and the back of the compressor.

The actual magnitude and the stage-wise distribution of rotor and stator loadings chosen for the final design resulted from a large number of iterations. These were required to meet the aggressive performance goal of design point polytropic efficiency and surge margin. Additional small corrections to stage-wise loadings and stage matching were introduced after completion of rig build 1 tests.

Both, the 9-stage E3E core compressor and the TP400 core compressor are highly loaded machines. The inlet Mach number and the static pressure rise was increased to levels well beyond the standard range of loadings usually used in civil engine applications.

As an example FIG 3 shows the distribution of rotor Mach number and the rotor static pressure rise coefficient versus relative length for the three compressors. Again, the BR700 figures represent the standard state-of-the-art level of loading. The E3E and TP400 rotor Mach numbers are well above those of the BR700 on all stages. The TP400 Mach number are plotted against E3E stages 3 to 8 to demonstrate the compressor family approach taken for the two designs, which is present throughout the full set of design parameters not shown here.

The E3E compressor has a variable IGV and variable stators 1 to 3. In particular these variable stages were found to have potential to take loadings up above BR700. Relative to BR700, static pressure rise coefficients were significantly increased across the front stages of the E3E compressor, while more similarity between BR700 and E3E was maintained in the rear stage block.

This is also true for the TP400 choice of static pressure rise coefficients, but these were taken even beyond the corresponding E3E figures due to different operability requirements on E3E and TP400. The engine performance cycle optimisation on the TP400 resulted in an HPC pressure ratio of 7, which represents a magnitude proposing a number of 1 to 2 variable vanes to be used on this compressor. Eventually the low-risk approach was taken and the 6-stage compressor was designed for having 2 variables (IGV and stator 1), allowing a more aggressive distribution of loadings across the front stages.

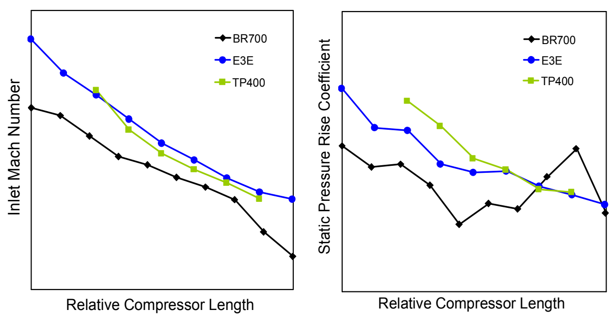

FIG 3. Stage-Wise Rotor Loading Distributions

3.3. Design Process and Numerical Modelling

At the start of the design process a parametric study was carried out using a meanline method to come up with adequate choices for the gas path, the number of stages, the distribution of stage pressure ratios, the distribution of stage reaction, the aerodynamic loading parameters and the number of aerofoils. This starting point of the design provides a good estimate of compressor efficiency and surge margin. Improvements achieved during the detailed design downstream in the process are fed back to the meanline model for re-assessment, see FIG 4.

The refinement of the flow path and the definition of the radial distribution of aerodynamic parameters was carried out using a throughflow method, which even today represents the backbone of the design systems. Based on boundary conditions given by the throughflow solution, a first set of aerofoil sections was automatically generated applying past experience design criteria. The blading generation block of the design process incorporates a blade-to-blade solver allowing to analyse the individual aerofoil sections with respect to their two-dimensional aerodynamic performance in the S1-plane.

Having designed the first set of annulus and aerofoil geometries a three-dimensional multi-stage CFD model of the compressor is generated to do an early assessment of the viscous flow, the stage matching and the resulting performance of the compressor. Initially the CFD model is based on assumptions and simplifications with respect to a number of geometric features along the boundaries of the flow path since the mechanical design had not progressed as far to give some representative input. Usually major weaknesses of the aerodynamic design are identified and corrective measures are taken introducing changes at the blading, the throughflow or even the meanline level of the design process. Depending on the design goal, this might be required more than one time.

At a certain stage of the design real-geometry features are known, such as the size and shape of bleed off-takes, aerofoil tip clearances, platform fillets, shroud wells and other gas-washed steps and gaps. Including these in the design iteration again may have an impact on the main design choices and the details of the blading since all of the real-geometry feature have a differently large but detrimental effect on the pressure rise capability and the efficiency of individual stages, and hence the overall performance of the compressor.

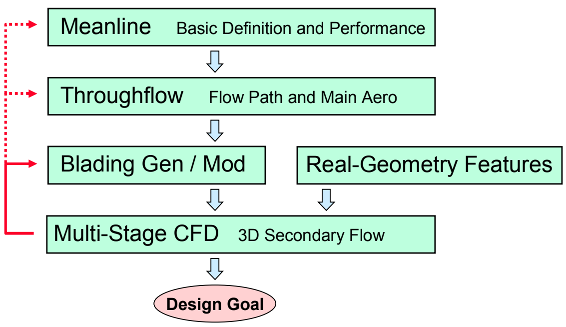

FIG 4. Design Process

Simulations of the steady, three-dimensional viscous flow field were carried out on the full compressor including the IGV, using the in-house 3D Navier-Stokes code Hydra for most of the design iterations and Numeca Fine Turbo for getting a second opinion on selected aspects of the design. The whole compressor is modelled in order to capture all radial and stage-wise matching effects, which occur in confined regions or even larger blocks of the compressor.

Hydra works unstructured, Numeca structured. Both CFD codes solve the Reynolds-averaged Navier-Stokes equations on multi-block grids, using mixing planes to connect individual blade rows. An explicit time marching, implicit residual smoothing 4-step Runge-Kutta procedure, and a cell-centered 2nd-order finite-volume discretisation is used. Multi-grid functionality improves convergence. The turbulence model of Spalart-Allmaras is usually employed in both codes.

The upper part of FIG 5 shows the full 9-stage CFD model of the E3E compressor and the predicted pressure field on the surfaces of the flow path at the design condition. This model was run through a variation of back pressures and rotational speeds to get an assessment across the entire operation envelope of the compressor. Overall characteristics and stage characteristics resulted from this exercise, which were repeatedly predicted during the progress of the design.

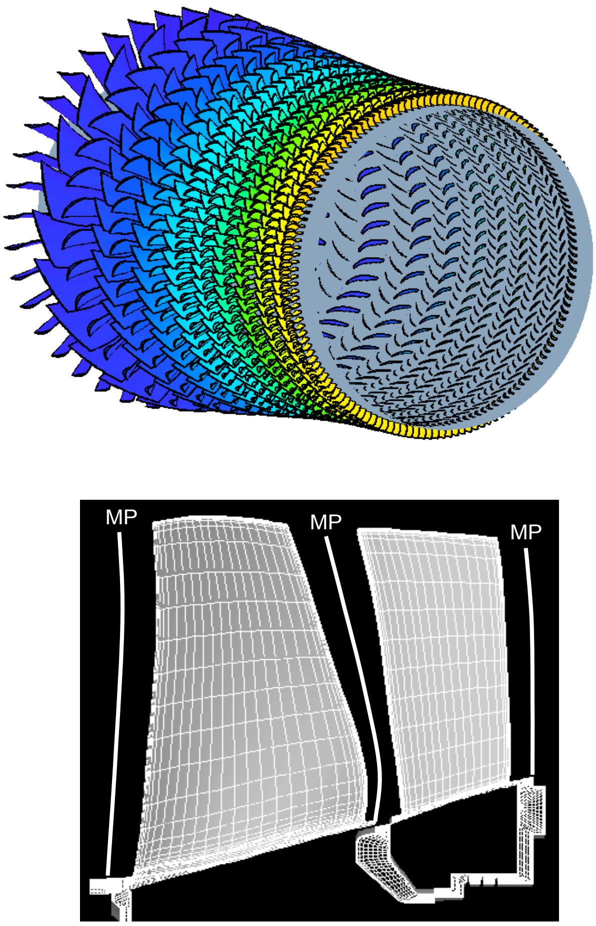

FIG 5. E3E Compressor Multi-Stage CFD Model

In the lower part of FIG 5 the compressor front stage is depicted to give an impression of the grid topology used. For the purpose of better visibility the grid shown is the lowest multi-grid level used within the calculations. The major portion of the blade passages was modelled using a standard elliptical H-grid. The number of cells in radial direction is above 70. The true tip geometry of rotors and cantilevered stator was modelled introducing separate tip clearance grid blocks with at least 13 cells in radial direction. On both, rotor and stator, a butterfly grid topology was used, which consists of an inner H-type core portion encapsulated by an O-type grid domain. Except in the region around the blade edges grid cell aspect ratios were kept below 8, expansion ratios below 10 and y+ below 8. The multi-stage model features mixing planes (MP) in each axial gap. A small cavity present in front of the rotor at the hub is partly meshed up to capture leakage flow entering the main flow path at this location. The shroud well geometry and the radial gaps occurring at the ends of the variable stator 1 in front of and behind the penny were included towards the end of the design.

The multi-stage CFD model was run at various off-design conditions to prove sufficient compressor stability and acceptable efficiency lapse rates towards high and part power operating conditions. FIG 6 shows the front stage operating de-throttled below the design point (DP) and throttled above the design point at a high position on the overall compressor characteristic.

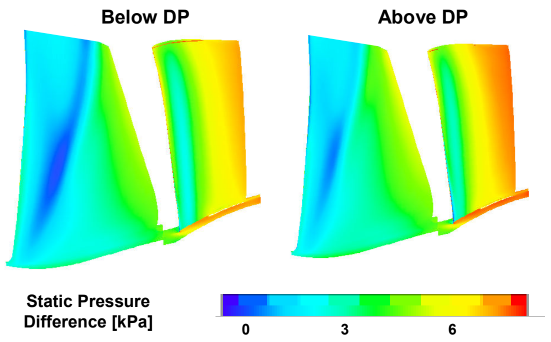

FIG 6. E3E Compressor Front Stage at Off-Design

3.4. Overall Performance Achievements

As a consequence of having introduced a significant step change in terms of applied aerodynamic design parameters relative to the technology used on the BR700 core compressor, the first build of the E3E compressor showed a number of deficiencies leading to a relatively low level of performance, which had to be addressed in a follow-on design iteration. The rig test data analysis and also a thorough CFD post-test analysis of the compressor showed insufficient matching of the front and rear stages. The importance of modelling a number of real-geometry details present along the boundaries of the main flow path, such as variable vane penny gaps, bleed off-takes, and stator shroud sealing was underestimated for the loading chosen for the design. Also the mechanical integrity of the rig part was poor, resulting in further performance deficiencies and an early failure of build 1.

After the strip of E3E rig build 1 the contributions causing the performance shortfall observed could be identified and investigated in depth using advanced steady-state and unsteady CFD modelling. One of the keys was proper accounting for real-geometry and secondary flow effects present on this highly loaded design. In combination with a number of additional aerodynamic technologies available through German and European research programmes the second design iteration eventually resulted in a successful build 2 of the E3E core compressor, which demonstrated a significant improvement in efficiency and surge margin. FIG 7 shows a comparison of working line polytropic efficiencies of a number of the different compressors. The E3E build 2 and the TP400 build 1 have improved relative to the BR700 HPC.

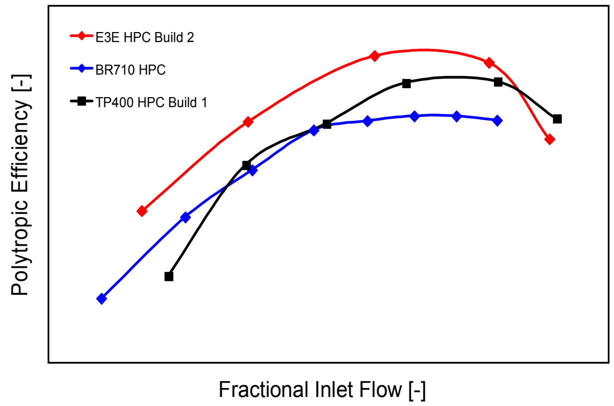

FIG 7. Efficiencies of Recent Rig Builds

Having learnt the lessons from the E3E compressor design exercises, the TP400 core compressor was developed in close analogy, using the established process and similar approaches to define flow path and blading. This compressor design was completed within short time scales, given the changes of design objectives being imposed during this phase. The validation plan for the TP400 compressor made provision for a series of two rig builds to demonstrate the expected performance. The level of efficiency and surge margin were found to be first-time-right on rig build 1 and exceeded the design goals given for this very challenging engine application. FIG 8 shows the good match of the high-speed compressor maps of TP400 and E3E when plotting characteristics in non-dimensionalised terms as fractions of their individual design figures.

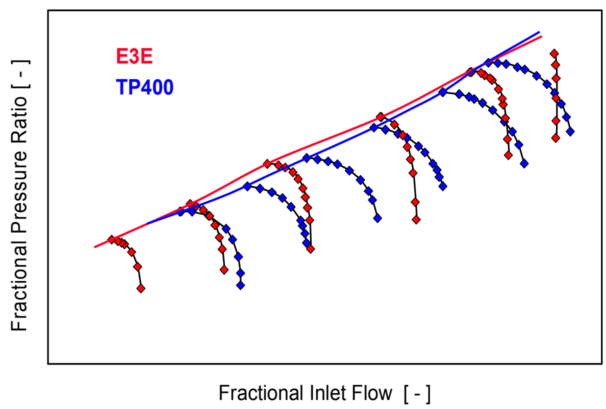

FIG 8. Normalised E3E and TP400 Compressor Map

4. TECHNOLOGY ATTRIBUTES

In support of the development of the E3E and TP400 compressor a number of smaller technology acquisition programmes have provided additional design attributes for the two compressors, which have taken efficiency and stability to the level demonstrated on the rigs. Some of these design attributes are discussed in the following paragraphs.

4.1. Swept Rotor Tip Design

The use of sweep and dihedral on rotors and stators is state of the art for most of todays compressor designs. The shape of modern aerofoil ranges from one hardly recognisable as being of 3D-style to one having extremely curved or bowed edges with occasionally strong local distortion. Most of these modern aerofoils are a product of empirically established improvements. The present 1st generation of 3D aerofoils certainly has potential for improvement, in particular with respect to the flow field in the region of radial gaps occurring at the tip of rotors or cantilevered stators. A analytical design methodology was developed allowing to identify the most effective 3D tip shape for any given aerofoil. FIG 9 shows a conventional 2D rotor and a 3D rotor featuring a tailored swept tip region. Both rotors are designed for low-speed research purposes at the same duty.

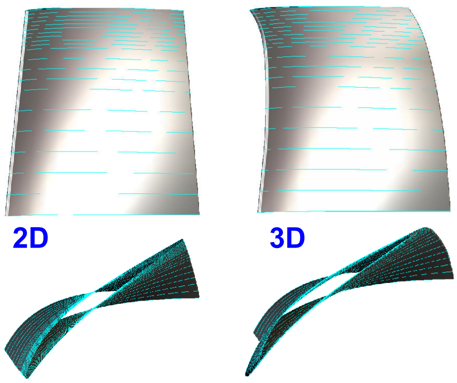

FIG 9. Conventional 2D Rotor and Swept 3D Rotor

A detailed CFD analysis of the flow field of the two rotors was conducted using a 3D Navier-Stokes code. The rotor was modelled in a multi-row environment with an IGV located upstream and a stator located downstream. The rotor domain was discretised using approximately 800.000 cells to give high resolution in the main flow field as well as in the tip gap region. Half of the number of cells was used on each of the stators. FIG 10 shows total pressure contours and streamlines of the three-dimensional flow field in the blade passage near the blade tip. On the 2D rotor the tip leakage vortex occurs close to the leading edge, where it immediately generates high losses. When travelling down the blade passage the small discrete spot of high loss grows into a loss region covering the full blade pitch. To some degree this is due to the behaviour of the tip leakage vortex, which slows down and looses its vortical characteristics already in the front portion of the blade passage. In the swept 3D rotor the tip leakage vortex is also originated near the leading edge, but the total pressure deficit generated along its way through the blade passage is significantly reduced relative to that occurring in the 2D rotors. All loss regions have reduced to almost half the size. The vortex has less blocking effect in the 3D rotor due a more streamwise orientation and it looses its vortical characteristics further downstream at about half-way down the passage rather than in the front of the passage.

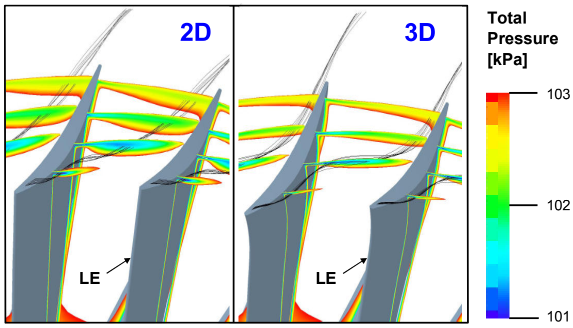

FIG 10. Total Pressure Contours and Streamlines, 2D and 3D Rotor Tip Region

FIG 11 shows contours of axial velocity in a blade-to-blade plane located at mid-gap height close to the casing for both rotors at design point condition. The flow enters the passage at uniform axial velocity and approaches a 3D separation line, which is originated at the suction side near the leading edge and ends at about 30% chord at the pressure surface of the adjacent blade. Downstream of the 3D separation line there is a region of much lower axial velocity, showing a reverse-flow patch originated along the suction surface. The qualitative flow pattern is similar in both rotors, but in the 3D rotor the 3D separation line is less pronounced and downstream of the 3D separation line a much smaller region of reverse flow occurs. The reverse-flow patch is still located near the suction surface, but has reduced by about 20% in pitch-wise direction. There is little reduction of extent in chord-wise direction, but the peak negative axial velocity occurring near the aerofoil suction side is much lower, indicating reduced generation of loss and blockage.

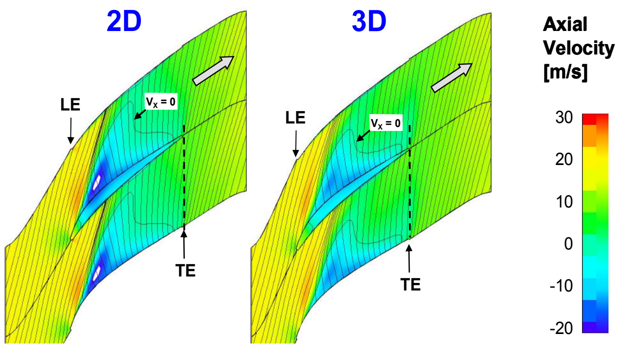

FIG 11. Axial Velocity Contours and Rotor-Relative Streamlines at Mid Tip Gap Height, 2D and 3D Rotor at Design Condition

4.2. Variable Vane Optimisation

Sufficient off-design operability of compressors of high pressure ratios is primarily achieved by the use of variable stator vanes, which feature a spindle on both of their ends to allow rotational movement. The angular travel range of the vanes can be as large as 50 to 60 degrees. The individual aerofoil ends are placed on so-called pennies, which usually have a diameter smaller than the actual chord length of the vane at the respective aerofoil end, see FIG 12. The result is a radial gap in the front, in the rear or on both sides of the penny, which have to be quite large in order to avoid contact of the aerofoil edges with the flow path contours when being rotated.

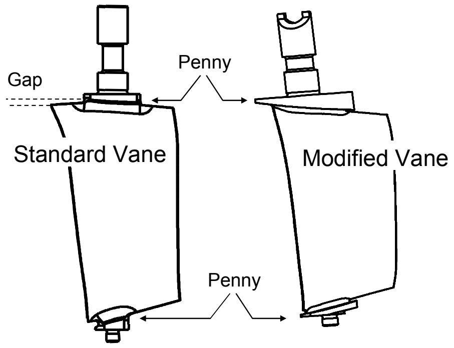

FIG 12. Standard and Modified Variable Stator Vane

The penny gaps are known to have a detrimental effect on the aerodynamic performance of the variable stator vanes. At moderate aerodynamic loading the losses generated by the gaps are acceptably low and for benefit of the mechanical design the spindle axis is usually placed in the vicinity of the centre of pressure of the aerofoil. At higher aerodynamic loading the relevance of the gaps was expected to increase, and a numerical and experimental study was carried out on a representative compressor cascade arrangement to investigate this. Three different configurations were considered, see FIG 13. The length of the front and rear gap were 21% and 25% of the aerofoil true chord, the radial gap height was 1% of the aerofoil true chord. Configuration 1 features both the front and the rear gap, configuration 2 only has the rear gap, and configuration 3 has no gap.

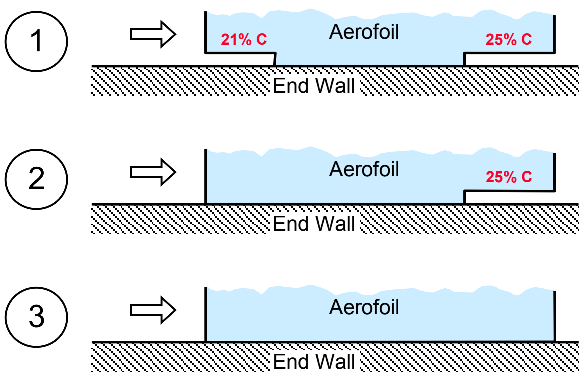

FIG 13. Penny Gap Configurations

All three configuration were modelled using a Rolls-Royce in-house 3D-Navier-Stokes code. FIG 14 shows the computational grid in the region near the end wall within the penny gap of configuration 1, featuring multi-block discretisation. O-grid topology is used in a narrow area around the aerofoil and within the gap, and H-blocks cover the main, the inlet and the outlet domain. The grid size is approximately 2.4 Mio cells.

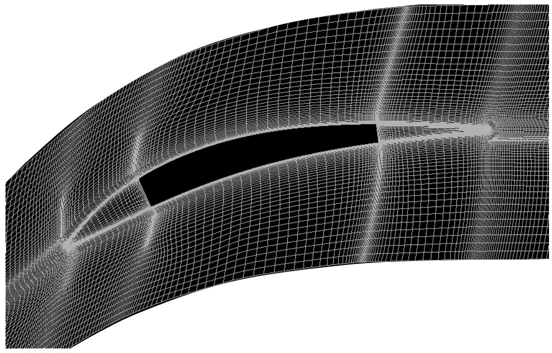

FIG 14. Computational Grid Near End Wall, Config. 1

The CFD simulations and the cascade experiments were carried out for the same range of inlet flow angle conditions. FIG 15 shows predicted and measured radial distributions of loss in the range between end wall and mid span for the design condition. CFD predicted huge losses occurring almost half-way towards mid span for Config. 1. Losses predicted for Config. 2 and 3 are very similar and drastically lower than those of Config. 1. Therefore, the front gap appears to generate the bulk of the losses, whereas the rear gap has much less impact on the performance of the vane. The test results confirm the radial extent and the qualitative pattern of the loss region, and also the similarity between Config. 2 and 3 predicted by CFD. However, the test shows larger losses across most of the end wall region. This is in particular the case for Config. 2 and 3, implying that the achievable benefit of removing the front gap is less than CFD predicts.

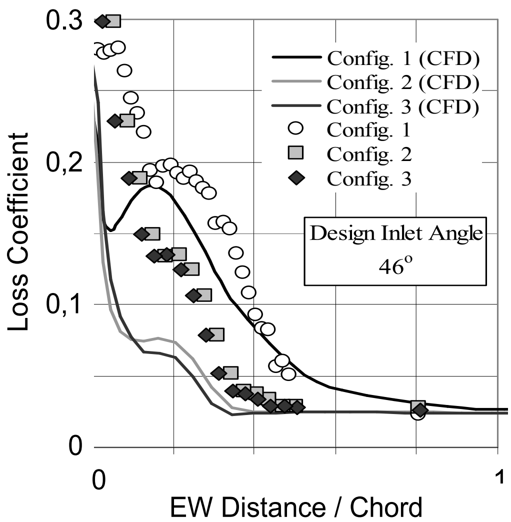

FIG 15. Radial Distribution of Loss, CFD and Experiment

4.3. Tailored Bleed Off-Takes

The standard way of taking bleed from compressors to supply engine secondary systems with pressurized air is through simple circular holes within the passage or through circumferential slots in the axial gap between two blade rows. Standard circular bleed holes are usually located in the rear part of the passage towards the pressure side of the aerofoil (region of maximum static pressure). In the reference case discussed here the off-take centre line is inclined against the radial direction by about 30° to ease flow entry, see FIG 16.

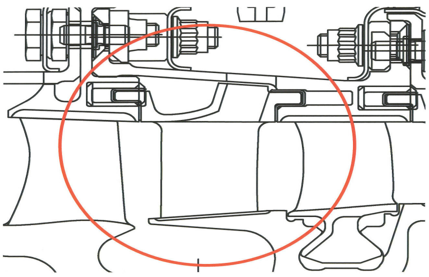

FIG 16. SAS Bleed Arrangements

This configuration was expected to give high bleed off-take pressures, but CFD simulations revealed large regions of separation and poor stator performance. FIG 17 shows the stator aerofoil and the casing end wall, viewed from the rear. Mach number contours and surface streaklines illustrate the intra-passage flow field. Blue colour designates regions of low-momentum flow. The corner stall in the circular off-take (OT) configuration is large and the surface streaklines show a pattern of 3D separation and attachment lines in the corner stall region, dominated by flow stagnation and reverse flow. On both, the hub and the suction surface, a focus occurs, indicating high flow path blockage and high entropy rise. In the remaining fraction of the pitch, which is not blocked by the corner stall, little end wall boundary layer leaves the passage. At mid-chord some boundary layer moves towards mid-span and feeds the corner stall, but at and beyond the bleed position the cross-passage flow mechanism is almost eliminated due to full removal of boundary layer there. The way the circular OT takes the air from the passage causes high diffusion in the end wall suction side corner and leads to growth of the corner.

In order to avoid the detrimental effects observed and based on knowledge about 3D flow in stators given in [9] and [10], the position and shape of the bleed off-take were tailored to fit the specific needs of the stator flow field. The tailored OT is also located in the casing end wall, but further downstream and closer to the aerofoil suction surface. This arrangement allows control of the corner stall region. The OT area is reduced and its shape was stretched in streamwise direction. Relative to the circular OT the flow field has drastically improved, see FIG 17. The streaklines show a 3D surface flow pattern in the suction side corner, which still features a separation line on the aerofoil, but - in contrast to normal corner stall topologies - shows associated secondary flows directed towards the casing end wall. The tailored OT removes less casing boundary layer at stator exit than the circular OT, but is able to capture the bulk of the cross-passage flow approaching the suction surface. The thickness of the hub boundary layer and therefore the hub blockage is larger than in the configuration with circular bleed off-take. The trailing edge wake is uniform across most of the stator span.

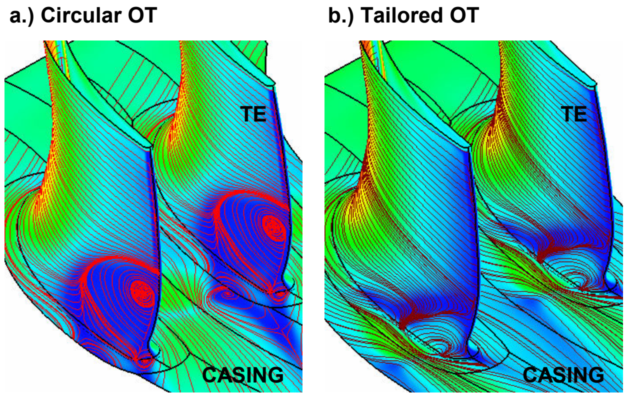

FIG 17. Surface Mach Number Contours and Streaklines

This is very clearly reflected in the pitchwise-averaged radial distribution of deviation and loss. FIG 18 shows these for the circular and the tailored OT, and also (for information only) a clean configuration without OT, all at the stator design operating condition. On the circular OT configuration the corner separation leads to high losses and to deviations of up to 16° in the outer half of the aerofoil. Introducing the tailored off-take gives a small increase in deviation in the inner half of span, including the hub tip clearance region, but a drastic improvement bringing deviation back to the design intent and strongly reducing losses across most of the annulus height. In contrast to the huge underturning found on the circular OT configuration a significant amount of overturning occurs on the tailored OT configuration in the outer 10% of annulus height.

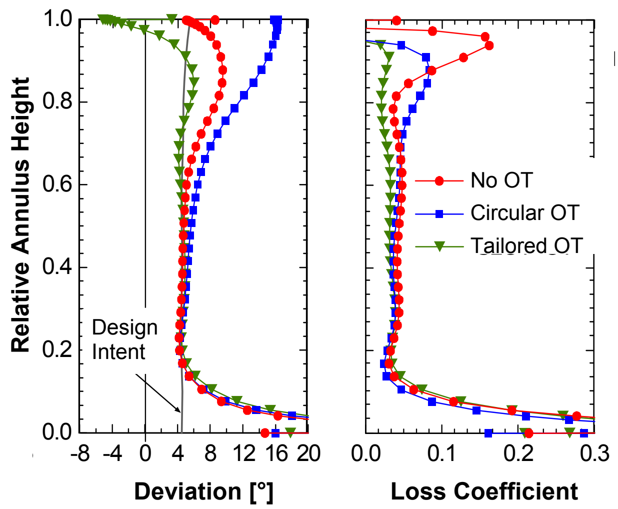

FIG 18. Radial Distribution of Stator Pitchwise-Averaged Deviation and Loss Coefficient

5. CONCLUSIONS

A new family of compressors has been developed incorporating novel aerofoil concepts and taking into account the strongly three-dimensional character of the flow field. In an approach of developing a compressor family for a range of various applications and pressure ratios, the TP400 and E3E core compressors were designed and tested.

Integrating the technology of these two machines allowed to achieved a pressure ratio and efficiency in only nine stages on the E3E compressor, which is unique for current designs.

Having set up the right design process and reflecting a sufficient level of detail in CFD predictions, such as features on the main flow path, on the blading and on any other gas-washed surface or cavities communicating with the main flow path, the number of design iterations to meet the design goals could be significantly reduced.

Backing up the design with innovative but close-to-product technology programmes allowed to successfully develop the E3E and TP400 compressor to the high level of performance demonstrated on the respective rig tests.

6. ACKNOWLEDGMENTS

The authors would like to thank the management of Rolls-Royce Deutschland Ltd. & Co. KG for supporting the work and permitting the presentation of results. The authors and Rolls-Royce gratefully acknowledge the support and funding contributions to the compressor development programme provided by Brandenburg State and the German Federal Government.

7. REFERENCES

[1] *Hobbs, D. E., Weingold, H. D., 1983*, "Development of Controlled Diffusion Airfoils for Multistage Compressor Application", ASME-Paper 83-GT-211.

[2] *Behlke, R. F., 1986*, "The Development of a Second Generation of Controlled Diffusion Airfoils for Multistage Compressors", Journal of Turbomachinery, Vol. 108 (1986), pp. 32-41.

[3] *Weingold, H. D., Neubert, R. J., Behlke, R. F., Potter, G. E., 1995*, "Reduction of Compressor Stator Endwall Losses Through the Use of Bowed Stators", ASME Paper 95-GT-380.

[4] *Gümmer, V., Wenger, U., Kau, H.-P,.2000,* “Using Sweep and Dihedral to Control Three-Dimensional Flow in Transonic Stators of Axial Compressor”, ASME-Paper 2000-GT-491.

[5] *Gallimore, S. J., Bolger, J. J., Cumpsty, N. A., Taylor, M. J., Wright, P. I., Place, J. M. M., 2002*, “The Use of Sweep and Dihedral in Multistage Axial Flow Compressor Blading, Part I: University Research and Methods Development”, ASME Paper GT-2002-30328.

[6] *Gallimore, S. J., Bolger, J. J., Cumpsty, N. A., Taylor, M. J., Wright, P. I., Place, J. M. M., 2002*, “The Use of Sweep and Dihedral in Multistage Axial Flow Compressor Blading, Part II: Low and High Speed Designs and Test Verification”, ASME Paper GT-2002-30329.

[7] *Kau, H.-P., 2002*, “Technologie und Auslegung des BR700 Hochdruckverdichters”, DGLR Jahrestagung, Paper 94-F4-102, pp. 649-655, September 1994.

[8] *Wenger, U., 2000,* “Anforderungen an die Verdichtertechnologie zur Unterstützung der nächsten BR700 Triebwerksgeneration”, DGLR Jahrestagung, Paper JT2000-106, pp. 1-4, September 2000.

[9] *Gbadebo, S. A.,Cumpsty, N. A., Hynes, T. P., 2004*, “Three-Dimensional Separations in Axial Compressors”, ASME Paper GT2004-53617.

[10] *Stratford, B. S., 1973*, “The Prevention of Separation and Flow Reversal in the Corner of Compressor Blade Cascades”, Technical Note, Aeronautical Journal, pp. 249-256, May 1973.